RSC Advances

PAPER

View Article Online
View Journal | View Issue

Cite this: *RSC Adv.*, 2025, **15**, 20464

Production and processing of zein nanoparticles as structural colorants†

Mia R. Wasilewski, Ji-Young Lee, Patrick A. Sullivan and Leila F. Deravi *

Received 2nd May 2025
Accepted 11th June 2025

DOI: 10.1039/d5ra03113c

rsc.li/rsc-advances

The emergence of structural coloration in nature requires precise control over material selection, processing, assembly, and distribution to create monodispersed nanostructured arrays. Such control has been historically difficult to replicate and scale for materials applications due to feedstock heterogeneity or complex assembly conditions. We explore the application and processing of an unconventional biomaterial, zein protein, as a template for structural coloration that may overcome these challenges. We leverage the spontaneous assembly of zein as nanoparticles using antisolvent precipitation to create structures with diameters ranging from 180 to 220 nm—a size regime that enables structural color formation. When cast as films, the nanoparticles produce amorphous coatings that display a reflectance peak at 410 nm indicative of violet-blue coloration, highlighting a unique avenue for these biomaterials as structural colorants.

1 Introduction

Structural coloration is dependent on the arrangement of nanostructures that interfere with specific wavelengths of visible light *via* multiple reflectance events.[1,2] This results in the selective cancellation or enhancement of specific visible wavelengths and is responsible for the production of vibrant colors or iridescence in nature.[3,4] Structural color phenomena are found in many organisms. Examples include the iridescent keratin-based lamellar structures of morpho butterfly wings, rod-shaped melanosomes in peacock feathers, and guanine crystals arrayed in chameleon iridophores.[5–8] The ability to replicate such phenomena using biologically derived or inspired structural colorants for materials applications offers environmental compatibility, resistance to fading, and long-term stability.[9,10] However, the process of replicating and scaling structural coloration is challenging to emulate.[11] It requires a pure feedstock and control over reaction dynamics to transform soluble precursors into monodispersed nanostructures that can be processed as films to produce discrete visible colors.[12]

In spite of these challenges, structural coloration has been achieved using nanocrystals from colloidal cellulose and chitin, as well as nanoparticles synthesized from lignin and synthetic melanin.[13–15] These systems are capable of producing color spanning the visible spectrum on the ~1 mm scale.[16–18] However, structural coloration from cellulose and chitin nanocrystals typically requires additional quenching steps with dialysis, and lignin nanoparticle formation involves extensive mixing protocols with organic solvents prior to formation.[19,20] Methods to simplify the production of biological nanomaterials from more complex feedstocks like heterogenous green tea extracts have also been explored with some success, although applications for structural coloration still remain elusive.[21] Inspired by these past reports, we explored the use of zein, a prolamin nitrogen storage protein derived from corn, as an alternative material for generating structural color. Due to its unique amino acid content and amphiphilic structure, zein can precipitate as submicron particles *via* anti-solvent precipitation[22–24] with notable applications ranging from agricultural products to targeted drug delivery.[25–27] Small (<100 nm) zein nanoparticles have also been explored as a diffuse white colorant;[28] however, their potential in structural color application has never been explored.

Building on the simplicity of the antisolvent precipitation process, we optimize and systematically evaluate the effects of zein concentration on nanoparticle diameter and polydispersity. We describe conditions that yield nanoparticles with diameters of 180–220 nm that remain stable for over 2 weeks in water under different storage conditions. We demonstrate applications of nanoparticles cast as amorphous films to produce violet-blue structural color with a reflectance peak centered at 410 nm. These colors are visible on both polystyrene and silicon substrates and persist over multiple weeks in air, indicating a versatile platform for producing structural colors from an unconventional biomaterial like zein.

2 Results and discussion

Zein nanoparticles (ZNPs) were precipitated when 1 mL of a 7.0% (w/v) solution of soluble protein (in 70% (v/v) ethanol) was dropped into 1 mL of Milli-Q water stirred at 750 rpm

Department of Chemistry and Chemical Biology, Northeastern University, Boston, MA 02115, USA. E-mail: l.deravi@northeastern.edu

† Electronic supplementary information (ESI) available. See DOI: https://doi.org/10.1039/d5ra03113c

(Fig. 1a). Before precipitation, the zein solution presented an absorption band from 300–500 nm (λ_{max} = 325 nm), with minimal absorbance from 500–800 nm. Upon precipitation, the suspended ZNPs produced a diffuse white appearance with a broadened absorbance spanning from 300–800 nm (λ_{max} = 312 nm), highlighting that the transformation was complete (Fig. 1b). During the ZNP optimization phase, we selected a drop rate of 100 μL min^{-1} of zein solution into Milli-Q water, as this maximized nanoparticle formation while minimizing aggregation. At drop rates above and below 100 μL min^{-1}, we noticed significant variability of sizes and structure formation (Fig. 1c–f). We also observed the production of smaller nanoparticles which ranged from 102–148 nm depending on drop rate (Fig. 1g).

To optimize for conditions that create structural coloration, we applied the Bragg-Snell Law to calculate the diameter bounds for visible color.[29] To do so, we first extrapolated the refractive index of the initial zein solution from the experimental data, yielding a value of 1.535 ± 0.013 (Fig. S1a†). Next, we determined ZNP diameters required for visible colors. Here, we assumed air is the surrounding medium, where nanoparticles are assembled optimally in a close-packed face-centered cubic (FCC) arrangement, with a packing volume fraction of 0.74. Based on these parameters, ZNPs with diameters of 175–350 nm would exhibit visible structural color (Fig. S1b†). To validate our predictions, we next explored experimental conditions to generate diameters in this range. Here, we varied the starting volume of the zein : ethanol solution from 0.25–1.00 mL dropped into a fixed volume (1 mL) of antisolvent. These varying volumes then generated suspensions containing 1.40–3.50% (w/v) of ZNPs with hydrodynamic diameters maximized for the 3.50% (w/v) condition (189.5 ± 5.2 nm; Fig. 2a). These ZNPs also exhibited a low polydispersity

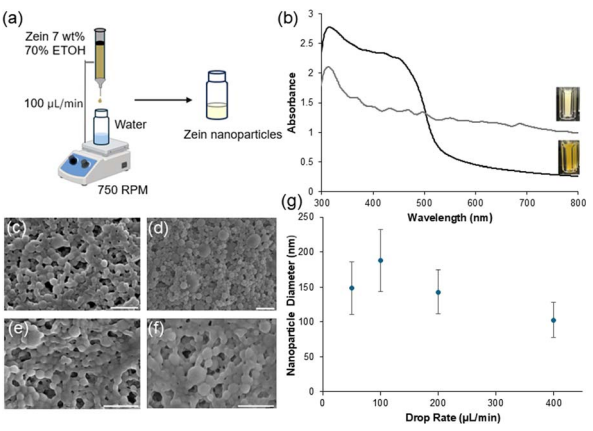

Fig. 1 (a) A schematic of the ZNP precipitation process. The zein : ethanol solution (1 mL) is dropped into the Milli-Q water antisolvent (1 mL), spinning at 750 rpm. (b) The absorbance spectrum of 7.0% (w/v) zein in 70% (v/v) ethanol prior to nanoparticle formation (black) and precipitated ZNPs at 3.50% (w/v) (grey). Representative SEM images of ZNPs formed at varying drop rates, (c) 50, (d) 100, (e) 200, and (f) 400 μL min^{-1}. All scale bars are 500 nm. (g) The nanoparticle diameters measured from N = 50 nanoparticles in the respective SEM images. Error bars are representative of standard deviation.

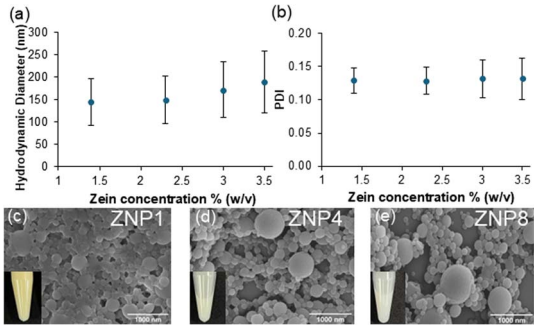

Fig. 2 Optimization of ZNP formation and drop-casting conditions. (a) Analysis of the hydrodynamic diameter of ZNPs at varying initial zein concentrations. (b) PDI analysis of ZNPs at varying concentrations. The size and PDI of all ZNP samples were measured using dynamic light scattering (DLS) in triplicate. (c–e) Representative SEM images of 3.50% (w/v) ZNPs at varying dilution factors (c) ZNP1 (1×) (d) ZNP4 (4×), and (e) ZNP8 (8×). Error bars are representative of the standard deviation.

index (PDI) of 0.13 ± 0.03, further supporting that the nanoparticles were mostly homogenous upon formation (Fig. 2b).

When evaluating the total solvent content, we calculated that this 3.50% (w/v) suspension (ZNP1) still contained 35% (v/v) ethanol. When cast as films on both silicon (Fig. S2a†) and polystyrene substrates (Fig. S2b†), these structures produced an opaque white color, with no notable reflectance signature (Fig. S2c and f†). We believe this opacity is likely due to nanoparticle aggregation as ethanol evaporates from the suspension (Fig. 2c). This may potentially be explained by van der Waals forces overcoming the initial electrostatic repulsion of the tightly packed ZNPs, which were further exacerbated by the high ethanol concentration. Higher ethanol concentrations might also increase the overall pH closer to zein's isoelectric point of 6.2, strengthening protein–protein interactions over nanoparticle repulsion during casting.[30] To test this hypothesis, we diluted the suspensions by 4× (ZNP4, Fig. 2d) and 8× (ZNP8, Fig. 2e) using Milli-Q water to effectively reduce the ethanol concentration to 8.75 and 4.37% (v/v) and lower pH from 4.16 to 3.80, respectively. When particles were diluted, aggregation seemed to diminish, and visibly separated particles were observed. These physical changes manifested as vibrant violet-blue colors with more prominent reflectance peaks when the particles were cast as films (Fig. S2c–h†). For instance, the reflectance spectra of the ZNP4 and ZNP8 films collected on both silicon and polystyrene substrates, displayed a distinct reflectance peak at 410 nm that intensified upon dilution with an overall increase of 13.8% from the 1× (ZNP1) to 8× (ZNP8) suspensions (Fig. S2a and b†). These data indicated that dilution improved short-range ordering required for the constructive interference of light.

We next assessed the stability of the suspended ZNPs in varying storage conditions. In these assessments, all nanoparticle suspensions were monitored at room temperature (25 °C), low temperature (4 °C), and high temperature (37 °C) conditions over two weeks using DLS (Fig. 3). At the highest concentration, ZNP1 aggregated then precipitated within the

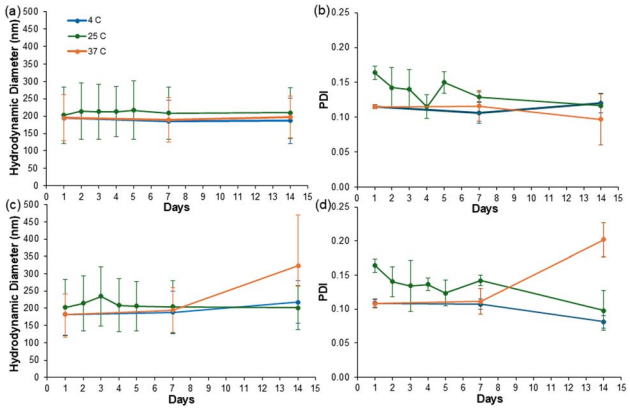

Fig. 3 The stability assessment of ZNP suspensions, where (a and b) ZNP4 and (c and d) ZNP8 conditions were monitored over a 14 day time period in low (4 °C, blue), ambient (25 °C, green), and high (37 °C, orange) temperature conditions. The values are averages from $N = 3$ samples, where error bars are standard deviation.

first 24 hours of analysis; thus, only ZNP4 and ZNP8 were monitored in this stability study. During the 14 day testing period, ZNP4 displayed minimal fluctuation in nanoparticle size across all conditions, with diameter changes of <11 nm from the starting nanoparticle size of 195 ± 1 nm (Fig. 3a) and minimal changes in PDI (Fig. 3b). This differed from the ZNP8 condition, which exhibited a ~20 nm diameter fluctuation under ambient conditions on day 3 and a subsequent increase of ~130 nm from day 7 to 14 in the 37 °C condition (Fig. 3c). ZNP8 also exhibited an increase in PDI of 0.09 ± 0.02 during this time (Fig. 3d). These data suggest the ZNP4 condition was the most stable in maintaining the nanoparticles in a uniform suspension under multiple storage environments. To determine whether films comprising these "aged" nanoparticles retained their violet-blue colors, we cast films using ZNP4 subjected to both high and low temperature conditions over 7 and 14 days. While there were small shifts across the CIELAB color space (Fig. S3a†), all films maintained their violet-blue colors (Fig. S3b–e†), supporting color stability under these conditions.

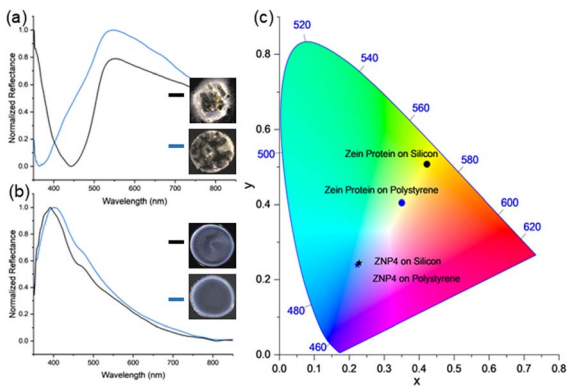

Fig. 4 The normalized reflectance of (a) dried zein protein prior to nanoparticle formation and (b) ZNP4 films on both silicon (black) and polystyrene substrates (blue) with their corresponding stereoscope images (inset). (c) The CIELAB diagram for zein powder before nanoparticle formation and ZNP4 on both silicon and polystyrene substrates.

With this information, we characterized ZNP4 on multiple substrates relative to the pre-precipitated zein solution. Here, the reflectance of zein before (Fig. 4a) and after (Fig. 4b) nanoparticle formation on both silicon and polystyrene was assessed. When drop-cast and dried, ZNP4 produced films with a thickness of ~ 2–4 μm (Fig. S4†). On both substrates, the ZNP4 films again presented a reflectance peak centered at 410 nm, which correlated to the violet-blue color space using the CIELAB conversion (Fig. 4c). This differed from the pre-precipitated zein solution (Fig. 4a), which demonstrated varying degrees of yellow colors (Fig. 4c). These data support that nanoparticle formation under our optimized conditions transformed zein coloration, highlighting its potential as a unique biomaterial for structural coloration.

3 Experimental details

3.1. Preparation of zein nanoparticles (ZNPs)

ZNPs were synthesized by fully dissolving zein powder (0.7 g, Acros Organics) in 70% (v/v) aqueous ethanol solution (10 mL) and vortex mixing. The solution was added dropwise to Milli-Q water (1 mL) at a 100 μL min^{-1} flow rate using a syringe pump with a 23-gauge, 1/2-inch needle. Nanoprecipitation occurred upon contact with the antisolvent, leading to the formation of ZNPs. The antisolvent was stirred at 750 rpm to prevent localized supersaturation and particle aggregation. Following nanoparticle formation, all dilutions were performed using Milli-Q water.

3.2. Measurements of the real part of the refractive index of zein

The real part of the refractive index (n_{eff}) was measured for zein dissolved in 70% (v/v) aqueous ethanol at varying concentrations using a refractometer (Anton Paar Abbemat 300, light wavelength 589 nm). Measurements were performed in triplicate at 25 °C. The n_{eff} increased with increasing zein volume fraction (Fig. S1a†). The refractive index of zein (n_{zein}) was extrapolated by the following equation.[13]

$$n_{eff}^2 = n_{ethanol}^2(1 - V_{zein}) + n_{zein}^2 V_{zein} \quad (1)$$

where V_{zein} and $n_{ethanol}$ are the volume fraction of zein protein and the real part of the refractive index of ethanol, respectively.

3.3. Structural reflectance wavelength calculations

The reflectance wavelength, representing the structural color peak of ZNPs with varying particle diameters, was estimated using the Bragg–Snell Law (Fig. S1b†).[31–34]

$$\lambda = \left(\frac{\pi}{3\sqrt{2}\phi}\right)^{1/3}\left(\frac{8}{3}\right)^{1/2} D\left\{n_{zein}^2\phi + n_{medium}^2(1-\phi)\right\}^{1/2} \quad (2)$$

where ϕ is the volume fraction of particles (0.74 for a FCC arrangement);[35] is the ZNP diameter; n_{zein} (=1.535) is the zein

protein refractive index; and n_{medium} (=1, air) is the refractive index of the surrounding medium.

3.4. Dynamic light scattering

The hydrodynamic diameter and PDI were measured in triplicate using DLS (Malvern Nano-ZS90). Each measurement was performed with 13 scans of 10 seconds each at 25 °C. Samples were diluted to prevent multiple scattering.

3.5. Scanning electron microscopy

SEM images were analyzed using a Field Emission SEM microscope (Hitachi S-4800). ZNP samples (5 μL) were drop-cast onto 5 × 5 mm silicon wafers (Ted Pella, INC) and placed on an aluminium SEM pin stub (Electron Microscopy Sciences) using carbon adhesive tape (Electron Microscopy Sciences). Samples were sputter-coated at 0.08 mbar and 20 mA for 40 seconds (Cressington 108 Auto) and imaged at 3.0–5.0 kV and 10.0 μA.

3.6. Cross-sectional SEM imaging

A ZNP4 film formed on a 5 × 5 mm silicon wafer was submerged in liquid nitrogen, freeze fractured, and analyzed on an aluminum SEM pin stub with a 90° cross-section holder (Electron Microscopy Sciences). The sample was sputter coated with ~10 nm of Pt. SEM imaging was performed at 3 kV and an 8 mm working distance using secondary electron imaging.

3.7. Optical measurements

The absorbance spectra of the zein : ethanol solutions and ZNPs were collected using a UV-visible spectrophotometer (Evolution 220, Thermo Scientific). Reflectance spectra were measured using a fiber optic probe connecting the UV-vis spectrophotometer (Ocean Optics, Flame UV-vis spectrometer) to a 20 W halogen light source.

3.8. Stereomicroscope imaging

Images of 10 μL ZNP drop-casts were captured using a stereomicroscope (SMZ18, Nikon) once fully dried on polystyrene Petri dishes and silicon wafers.

4 Conclusions

In this study, we developed a method to produce ZNPs with sufficiently large particle diameters (180–220 nm) to support applications in structural coloration. Unlike other biomaterials capable of being processed as structural colors, production of ZNPs is accomplished within 20 minutes through a single-step precipitation method, without the need for surfactants or additional purification steps. This differs from production of chitin[19] and cellulose[14] nanocrystals, which undergo dialysis processes that are multiple days long. Lignin[18] and synthetic melanin[13] nanoparticle formation similarly requires longer processing times, including a multistep mixing process which happens over several hours.

Through our optimization of antisolvent precipitation, we show how initial ZNP suspensions, presenting an overall white color dominated by broadband light scattering, can be transformed to films presenting violet-blue colors due to Bragg-based structural coloration. Future work will explore experimental conditions (*i.e.*, needle diameter, vessel volume, and/or order of addition) to diversify the particle size and subsequent visible colors accessible from this process. While theoretically feasible (Fig. S1†), we anticipate some experimental challenges associated with manufacturing larger sizes. Because ZNP formation is a diffusion-driven precipitation, it may become more difficult to maintain a low PDI at larger particle sizes due to an increased likelihood of secondary aggregation. Additionally, larger particles may experience stronger van der Waals interactions during film formation, increasing the risk of irregular packing or phase separation, both of which could suppress structural color. These challenges may be offset with additives, like surfactants, to suppress aggregation during film formation. For now, our data highlight the rich potential for prolamin proteins as alternative materials that should continue to be explored for structural coloration.

Data availability

The data supporting this article have been included as part of the ESI.†

Conflicts of interest

There are no conflicts to declare.

Author contributions

Mia Wasilewski and Leila Deravi designed and performed experimentation and wrote the manuscript; Ji-Young Lee performed theoretical calculations and revised the manuscript; Patrick Sullivan designed the preliminary experiments; all authors have given approval to the final version of the manuscript.

Acknowledgements

The authors gratefully acknowledge support from the Department of Chemistry and Chemical Biology at Northeastern University and past contributions from Chloe Sivitz, Ivy Wang, and Dr Duncan Bower. The authors would also like to thank Dr Shirin Kaboli and the Boston Electron Microscopy Center Facility for their help in the SEM analysis.

References

1 A. Kawamura, M. Kohri, G. Morimoto, Y. Nannichi, T. Taniguchi and K. Kishikawa, *Sci. Rep.*, 2016, **6**, 33984.
2 C. Finet, *Humanit. Soc. Sci. Commun.*, 2023, **10**, 348.
3 J. Sun, B. Bhushan and J. Tong, *RSC Adv.*, 2013, **3**, 14862–14889.
4 Y. Zhao, Z. Xie, H. Gu, C. Zhu and Z. Gu, *Chem. Soc. Rev.*, 2012, **41**, 3297–3317.

5 L. Feng, F. Wang, H. Luo and B. Qiu, *Dyes Pigm.*, 2023, **210**, 111019.
6 R. H. Siddique, S. Diewald, J. Leuthold and H. Hölscher, *Opt. Express*, 2013, **21**, 14351–14361.
7 G. Isapour and M. Lattuada, *Adv. Mater.*, 2018, **30**, 1707069.
8 J. Teyssier, S. V. Saenko, D. van der Marel and M. C. Milinkovitch, *Nat. Commun.*, 2015, **6**, 6368.
9 N. Echegaray, N. Guzel, M. Kumar, M. Guzel, A. Hassoun and J. M. Lorenzo, *Food Chem.*, 2023, **404**, 134453.
10 A. Tittl, *Light: Sci. Appl.*, 2022, **11**, 155.
11 J. B. Kim, S. Y. Lee, J. M. Lee and S.-H. Kim, *ACS Appl. Mater. Interfaces*, 2019, **11**, 14485–14509.
12 K. Li, C. Li, H. Li, M. Li and Y. Song, *iScience*, 2021, **24**, 102121.
13 M. Xiao, Y. Li, M. C. Allen, D. D. Deheyn, X. Yue, J. Zhao, N. C. Gianneschi, M. D. Shawkey and A. Dhinojwala, *ACS Nano*, 2015, **9**, 5454–5460.
14 M. S. Reid, M. Villalobos and E. D. Cranston, *Langmuir*, 2017, **33**, 1583–1598.
15 J. Liu, M. Nero, K. Jansson, T. Willhammar and M. H. Sipponen, *Nat. Commun.*, 2023, **14**, 3099.
16 B. Frka-Petesic, T. G. Parton, C. Honorato-Rios, A. Narkevicius, K. Ballu, Q. Shen, Z. Lu, Y. Ogawa, J. S. Haataja, B. E. Droguet, R. M. Parker and S. Vignolini, *Chem. Rev.*, 2023, **123**, 12595–12756.
17 G. Zhao, S. Zhang, S. Zhai and M. Pan, *J. Mater. Sci.*, 2020, **55**, 8756–8767.
18 J. Wang, J. Lai, W. Zhao, C. Zhou and C. Hu, *Chem. Eng. J.*, 2024, **499**, 156362.
19 A. Narkevicius, R. M. Parker, J. Ferrer-Orri, T. G. Parton, Z. Lu, G. T. van de Kerkhof, B. Frka-Petesic and S. Vignolini, *Adv. Mater.*, 2022, **34**, e2203300.
20 Y. Habibi, L. A. Lucia and O. J. Rojas, *Chem. Rev.*, 2010, **110**, 3479–3500.
21 W.-T. Chang, J.-Y. Lee and L. F. Deravi, *ACS Omega*, 2025, **10**, 3930–3936.
22 N. Parris and L. C. Dickey, *J. Agric. Food Chem.*, 2001, **49**, 3757–3760.
23 S. Yang, M. Zheng, S. Li, Y. Xiao, Q. Zhou and J. Liu, *Food Sci. Technol.*, 2020, **40**(118), 106789.
24 E. Oleandro, M. Stanzione, G. G. Buonocore and M. Lavorgna, *Nanomaterials*, 2024, **14**(5), 414.
25 I. De Marco, *Polymers*, 2022, **14**, 2172.
26 S. Tortorella, M. Maturi, V. Vetri Buratti, G. Vozzolo, E. Locatelli, L. Sambri and M. Comes Franchini, *RSC Adv.*, 2021, **11**, 39004–39026.
27 E. A. Hanna, O. E. Mendez Lopez, F. Salinas, C. E. Astete, C. Tamez, Y. Wang, H. Wu, B. D. Eitzer, W. H. Elmer, S. Louie, J. C. White and C. M. Sabliov, *ACS Agric. Sci. Technol.*, 2022, **2**, 1013–1022.
28 F. Y. de Boer, R. N. U. Kok, A. Imhof and K. P. Velikov, *Soft Matter*, 2018, **14**, 2870–2878.
29 G. Mayonado, S. Mian, V. Robbiano and F. Cacialli, *Investigation of the Bragg-Snell Law in Photonic Crystals*, 2015.
30 M. Keramat, N. Kheynoor and M.-T. Golmakani, *Food Chem.:X*, 2022, **14**, 100279.
31 J.-H. Kim, J.-Y. Lee, J. Kim, Z. Gong, D. J. Wilson, L. F. Deravi and D. Lee, *J. Mater. Chem. C*, 2024, **12**, 2148–2155.
32 S. J. Yeo, F. Tu, S.-h. Kim, G.-R. Yi, P. J. Yoo and D. Lee, *Soft Matter*, 2015, **11**, 1582–1588.
33 T. M. Choi, J.-G. Park, Y.-S. Kim, V. N. Manoharan and S.-H. Kim, *Chem. Mater.*, 2015, **27**, 1014–1020.
34 P. A. Rundquist, P. Photinos, S. Jagannathan and S. A. Asher, *J. Chem. Phys.*, 1989, **91**, 4932–4941.
35 R. K. Cersonsky, G. van Anders, P. M. Dodd and S. C. Glotzer, *Proc. Natl. Acad. Sci. U. S. A.*, 2018, **115**, 1439–1444.